Spin-phonon interactions on the kagome lattice: Dirac spin liquid versus valence-bond solids

Francesco Ferrari,[1] Federico Becca,[2] and Roser Valentí[1]
[1]*Institute for Theoretical Physics, Goethe University Frankfurt, Max-von-Laue-Straße 1, D-60438 Frankfurt a.M., Germany*
[2]*Dipartimento di Fisica, Università di Trieste, Strada Costiera 11, I-34151 Trieste, Italy*

(Received 20 November 2023; accepted 1 April 2024; published 17 April 2024)

We investigate the impact of spin-phonon coupling on the $S = 1/2$ Heisenberg model on the kagome lattice. For the pure spin model, there is increasing evidence that the low-energy properties can be correctly described by a Dirac spin liquid, in which spinons with a conical dispersion are coupled to emergent gauge fields. Within this scenario, the ground-state wave function is well approximated by a Gutzwiller-projected fermionic state [Ran, Hermele, Lee, and Wen, Phys. Rev. Lett. **98**, 117205 (2007)]. However, the existence of $U(1)$ gauge fields may naturally lead to instabilities when small perturbations are included. Phonons are ubiquitous in real materials and may play a relevant role in the determination of the actual physical properties of the kagome antiferromagnet. Therefore, we perform a step forward in this direction, including phonon degrees of freedom (at the quantum level) and applying a variational approach based upon Gutzwiller-projected fermionic *Ansätze*. Our results suggest that the Dirac spin liquid is *stable* for small spin-phonon couplings, while valence-bond solids are obtained at large couplings. Even though different distortions can be induced by the spin-phonon interaction, the general aspect is that the energy is lowered by maximizing the density of perfect hexagons in the dimerization pattern.

DOI: 10.1103/PhysRevB.109.165133

I. INTRODUCTION

One of the longest-standing debates in the field of frustrated magnetism and quantum spin liquids concerns the ground state of the spin-1/2 antiferromagnetic Heisenberg model on the kagome lattice [1]. Drawing from early numerical evidence of the absence of long-range magnetic order [2–4], several theoretical predictions have been put forward, based on approximations and numerical methods of different kinds. The possibility of a (gapped) quantum spin-liquid ground state, derived from a large-N expansion based upon groups with symplectic $Sp(N)$ symmetry, was originally proposed in Ref. [5]. On the other hand, the (fermionic) $SU(N)$ approximation adopted in Ref. [6] pointed toward the existence of a dimerized ground state, characterized by the largest possible density of *perfect hexagons*, i.e., hexagonal plaquettes with three singlets. The valence-bond ordered picture was further corroborated by the results of other numerical methods, e.g., series expansion and quantum dimer models, which identified a dimerized ground state with a supercell of 36 sites and a honeycomb-like arrangement of perfect hexagons as energetically most favorable [7–9]. This conclusion was strengthened by the calculations of low-lying excitations above the valence-bond ordered ground state [10,11], which reproduced some of the features observed in exact diagonalization calculations on small clusters, most notably the large density of singlet excitations below the triplet gap [12–15]. Interestingly, within a short-range valence-bond basis, the lowest-energy singlet excitations were found to be the dimer coverings possessing a large number of perfect hexagons [16].

More recently, the valence-bond ordered scenario was challenged by various methods, e.g., density-matrix renormalization group (DMRG) [17–19] and variational Monte Carlo [20], which found a quantum spin liquid ground state in large-scale calculations. Within the latter approach, the best variational *Ansatz* was found to be a $U(1)$ Dirac state, namely a spin liquid with conical points in the spinon spectrum and emergent $U(1)$ gauge fields in the low-energy theory [21,22]. This state, described by a Gutzwiller-projected fermionic wave function, was shown to be stable to gap-opening instabilities, such as dimerization [23] and the lowering of the $U(1)$ gauge structure to Z_2 [24].

The presence of a Dirac spin liquid ground state is further supported by recent state-of-the-art numerical results. Indeed, although the first DMRG studies indicated the presence of a gapped spectrum [17–19], more recent calculations on infinitely long cylinders revealed the existence of Dirac spinons by means of adiabatic flux insertion [25,26], which helped in identifying fingerprints of gapless excitations that are gapped by the cylindrical geometry [27]. Furthermore, recent tensor-network calculations also corroborated the gapless nature of the spin-liquid ground state [28].

From a theoretical perspective, the stability of $U(1)$ Dirac spin liquids is enhanced on nonbipartite geometries, such as the kagome lattice [29]. Still, the Dirac spin liquid represents the parent state of certain proximate orders, namely magnetic and valence-bond solid phases, which can result from the condensation of monopoles with specific quantum numbers [29–32]. These instabilities can be triggered by deviations from the ideal nearest-neighbor kagome antiferromagnet, e.g., by the inclusion of longer-range exchange interactions [33–37]. In this regard, a theoretically and experimentally relevant question concerns the possible spin-Peierls instability of the Dirac spin-liquid state in the presence of a coupling between spins and lattice distortions (phonons). Indeed, in one dimension, the gapless spin-liquid ground state of the

Heisenberg chain is known to be unstable towards dimerization when spins are coupled to *static* lattice distortions [38,39]; however, when phonon degrees of freedom are treated *dynamically*, the spin-liquid phase remains stable below a finite critical value of the spin-phonon coupling [40–43]. In two dimensions, the situation is less understood and only a smaller number of works have focused on the impact of the spin-phonon coupling on spin-liquid phases. For what concerns Z_2 spin liquids, there are studies addressing detectable signatures of spin-lattice coupling in the phonon dynamics of the Kitaev spin liquid [44–46]. Furthermore, the phonon-driven transition between the Z_2 Dirac spin liquid phase on the square lattice and a dimerized phase has been assessed by us in Ref. [47]. On the kagome lattice, the spin-Peierls transition has been discussed only in the case of large magnetic fields for exact eigenstates with localized magnons [48]. However, the question of the stability of the kagome Dirac spin liquid to lattice distortions has not been addressed so far. Its proximity to several competing orders within a small energy range [15] may be interpreted as a sign of potential fragility towards dimerization. In relation to this, a recent field theoretical study identified a symmetry-allowed coupling between lattice distortions and monopole operators of the $U(1)$ Dirac spin liquid on the triangular lattice as a possible mechanism driving a spin-Peierls transition [49].

Motivated by these observations, we employ a variational Monte Carlo technique to investigate the ground-state properties of a spin-phonon Hamiltonian on the kagome lattice, treating the full quantum dynamics of both spins and phonons. We explore several channels of instability of the $U(1)$ Dirac spin liquid towards dimerization, which encompass also valence-bond ordered phases associated with its monopole operators [29]. The results of our study indicate that the $U(1)$ Dirac spin liquid is stable, i.e., a (first-order) spin-Peierls transition is found to take place only for finite values of the spin-phonon coupling. Then, the valence-bond solids favored by the spin-lattice interactions are those that maximize the number of rotationally symmetric hexagonal plaquettes with strong singlet correlations on their edges.

II. MODEL AND METHOD

We consider a system of localized $S = 1/2$ spins on the kagome lattice, which are coupled at nearest neighbors by the antiferromagnetic Heisenberg interaction J. The spin-phonon effects due to lattice distortions are modeled by assuming that the exchange coupling among the spins depends linearly on site displacements. The system is thus described by the following Su-Schrieffer-Heeger [50] Heisenberg Hamiltonian:

$$\mathcal{H} = \mathcal{H}_{\text{sp}} + \mathcal{H}_{\text{ph}}, \tag{1}$$

$$\mathcal{H}_{\text{sp}} = J \sum_{\langle i,j \rangle} \left[1 - g \frac{\vec{r}_i - \vec{r}_j}{\|\vec{r}_i - \vec{r}_j\|} \cdot (\vec{U}_i - \vec{U}_j) \right] \mathbf{S}_i \cdot \mathbf{S}_j, \tag{2}$$

$$\mathcal{H}_{\text{ph}} = \frac{\omega}{4} \sum_j \left(\vec{P}_j^2 + \vec{U}_j^2 \right). \tag{3}$$

Here $\mathbf{S}_j = (S_j^x, S_j^y, S_j^z)$ denotes the spin operator at site j. The lattice degrees of freedom are described by a set of local harmonic oscillators through the displacement and momentum operators, $\vec{U}_j = (X_j, Y_j)$ and $\vec{P}_j = (P_j^X, P_j^Y) = -2i(\partial_{X_j}, \partial_{Y_j})$. Within this notation [43,47], the canonical commutation relations between phonon operators become $[X_j, P_l^X] = [Y_j, P_l^Y] = 2i\delta_{j,l}$ (all other commutators vanish). The strength of the spin-phonon coupling is controlled by the adimensional constant g. The vector $\vec{r}_i = (x_i, y_i)$ marks the position of site i in the undistorted kagome lattice, and $\|\cdot\|$ denotes the Euclidean norm. The form of the spin-phonon coupling in $\mathcal{H}_{\text{sp}}$ arises from the linear term in the Taylor expansion of the exchange interaction as a function of the Euclidean distance between sites. The second term of Eq. (1), $\mathcal{H}_{\text{ph}}$, is the free Hamiltonian of Einstein (optical) phonons, i.e., uncoupled harmonic oscillators with a flat dispersion with frequency ω.

We notice that the model of Eq. (1) is invariant under the transformation $g \mapsto -g$ and $\vec{U}_j \mapsto -\vec{U}_j$ for all the sites j; thus, the sign of g does not affect the ground-state energy and the phase diagram. Here, we take $g > 0$, which corresponds to the more physical situation in which negative spin-spin correlations (e.g., singlet states) tend to shrink bonds, or, in other words, in which the exchange coupling decreases when spins are pulled far apart.

A. Variational wave function

We make use of a variational Monte Carlo method to approximate the ground-state wave function of the spin-phonon problem (1) on finite-size clusters with N sites and periodic boundary conditions. Our variational *Ansatz* is the product of a spin state $|\Psi_s\rangle$, a phonon state $|\Psi_p\rangle$, and a Jastrow factor $\mathcal{J}_{sp}$, which correlates spins with lattice distortions [43,47,51]:

$$|\Psi_{\text{var}}\rangle = \mathcal{J}_{sp} |\Psi_p\rangle \otimes |\Psi_s\rangle. \tag{4}$$

The variational energy E_{var} is estimated by performing a Markov process in the total Hilbert space that includes spin and phonon configurations $|\vec{u}; s^z\rangle = \bigotimes_j (|\vec{u}_j\rangle \otimes |s_j^z\rangle)$, i.e., in the local eigenbasis of the $\vec{U}_j$ (phonon) and S_j^z (spin) operators for each lattice site j [43]. Then, we have

$$\begin{aligned} E_{\text{var}} &= \frac{\langle \Psi_{\text{var}} | \mathcal{H} | \Psi_{\text{var}} \rangle}{\langle \Psi_{\text{var}} | \Psi_{\text{var}} \rangle} \\ &= \sum_{s^z} \int d\vec{u} \underbrace{\frac{|\langle \vec{u}; s^z | \Psi_{\text{var}} \rangle|^2}{\langle \Psi_{\text{var}} | \Psi_{\text{var}} \rangle}}_{\mathcal{P}(\vec{u}; s^z)} \underbrace{\frac{\langle \vec{u}; s^z | \mathcal{H} | \Psi_{\text{var}} \rangle}{\langle \vec{u}; s^z | \Psi_{\text{var}} \rangle}}_{e_L(\vec{u}; s^z)}, \end{aligned} \tag{5}$$

where the sum is over all spin configurations, and the integral is over all phonon displacements. Then, along the Markov chain, a set of configurations $(\vec{u}; s^z)_m$ (with $m = 1, \ldots, M$) are drawn according to the probability $\mathcal{P}(\vec{u}; s^z)$ and the Metropolis algorithm, which allows us to estimate the variational energy as

$$E_{\text{var}} \approx \frac{1}{M} \sum_{m=1}^{M} e_L(\vec{u}; s^z)_m. \tag{6}$$

The stochastic process is performed in the subspace of zero total spin along z, and the Metropolis moves for the spins involve nearest-neighbor double spin-flips; for the phonon degrees of freedom, the Metropolis moves consist of local updates of the displacements, $X_j \mapsto X_j + \Delta$ or $Y_j \mapsto Y_j +$

Δ, with Δ uniformly distributed within a certain interval $[-\Delta_{\max}, \Delta_{\max}]$.

The form of the variational state is partially dictated by the efficiency in the calculation of its amplitudes $\langle \vec{u}; s^z | \Psi_{\rm var} \rangle$. In this respect, the spin-phonon Jastrow factor must be diagonal in the chosen computational basis (otherwise it would require the calculations of matrix elements with all states of the basis). Therefore, we are limited to consider terms involving the z-component of the spin operators, thus breaking the SU(2) symmetry, and we take [43]

$$\mathcal{J}_{sp} = \exp\left[\frac{1}{2}\sum_{i,j} \vec{v}_{sp}(i,j)\cdot(\vec{U}_i - \vec{U}_j) S_i^z S_j^z\right], \tag{7}$$

where the pseudopotential parameters (antisymmetric under the exchange of i and j indices) are defined as

$$\vec{v}_{sp}(i,j) = \begin{pmatrix} v_{sp}^X(\|\vec{r}_i - \vec{r}_j\|)\frac{x_i - x_j}{\|\vec{r}_i - \vec{r}_j\|} \\ v_{sp}^Y(\|\vec{r}_i - \vec{r}_j\|)\frac{y_i - y_j}{\|\vec{r}_i - \vec{r}_j\|} \end{pmatrix}. \tag{8}$$

Then, given the *Ansatz* of Eq. (4), we have that

$$\langle \vec{u}; s^z | \Psi_{\rm var} \rangle = J_{sp}(\vec{u}; s^z)\, \langle \vec{u} | \Psi_p \rangle\, \langle s^z | \Psi_s \rangle, \tag{9}$$

where $J_{sp}(\vec{u}; s^z)$ is the value that the operator $\mathcal{J}_{sp}$ acquires on the configuration $|\vec{u}; s^z\rangle$. The phonon part of the variational *Ansatz* is a coherent state:

$$\langle \vec{u} | \Psi_p \rangle = \prod_i \exp\left(-\frac{\|\vec{u}_i - \vec{z}_i\|^2}{4}\right), \tag{10}$$

which is written as a product of Gaussians that are centered in the displaced positions of the lattice sites, represented by the variational parameters $\vec{z}_i = (z_i^X, z_i^Y)$. In general, nonzero values of $\vec{z}_i$ induce the presence of finite lattice distortion. Finally, the spin part of the variational state is defined within the Abrikosov fermion representation of $S = 1/2$ spin operators [52,53],

$$\mathbf{S}_i = \frac{1}{2}\sum_{\sigma,\sigma'} c_{i,\sigma}^\dagger \boldsymbol{\sigma}_{\sigma,\sigma'} c_{i,\sigma'}, \tag{11}$$

where $c_{i,\sigma}$ ($c_{i,\sigma}^\dagger$) is the annihilation (creation) operator of a fermion at site i with spin $\sigma = \uparrow, \downarrow$, and $\boldsymbol{\sigma} = (\sigma_x, \sigma_y, \sigma_z)$ is a vector of Pauli matrices. The state $|\Psi_s\rangle$ consists of a fermionic Slater determinant, $|\Phi_0\rangle$, which is projected onto spin space by the Gutzwiller operator $\mathcal{P}_G = \prod_i (2 - n_i) n_i$, where $n_i = \sum_\sigma c_{i,\sigma}^\dagger c_{i,\sigma}$, and supplemented by a spin Jastrow factor $\mathcal{J}_{ss}$ (diagonal in the computational basis):

$$|\Psi_s\rangle = \mathcal{J}_{ss}\mathcal{P}_G |\Phi_0\rangle. \tag{12}$$

We define $|\Phi_0\rangle$ as the ground state of an auxiliary tight-binding Hamiltonian on the kagome lattice, with nearest-neighbor hopping terms

$$\mathcal{H}_0 = \sum_{\langle i,j\rangle}\sum_\sigma t_{i,j} c_{i,\sigma}^\dagger c_{j,\sigma} + \text{H.c.}, \tag{13}$$

and the Jastrow factor as

$$\mathcal{J}_{ss} = \exp\left[\frac{1}{2}\sum_{i,j} v_{ss}(\|\vec{r}_i - \vec{r}_j\|) S_i^z S_j^z\right]. \tag{14}$$

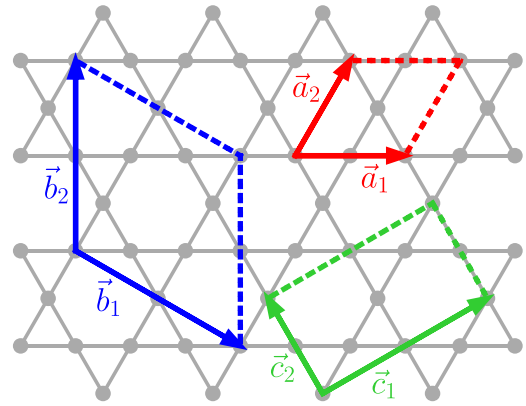

FIG. 1. Lattice vectors employed to construct different supercells for the variational *Ansätze*. Taking the nearest-neighbor distance as unit, the red vectors are defined as $\vec{a}_1 = (2, 0)$ and $\vec{a}_2 = (1, \sqrt{3})$ (primitive vectors). The blue vectors are $\vec{b}_1 = 2\vec{a}_1 - \vec{a}_2$ and $\vec{b}_2 = 2\vec{a}_2 - \vec{a}_1$. The green vectors are $\vec{c}_1 = \vec{a}_1 + \vec{a}_2$ and $\vec{c}_2 = \vec{a}_2 - \vec{a}_1$.

The Gutzwiller projection is implemented by the Markov chain, in which spin configurations are sampled, i.e., fermionic configurations with singly occupied sites. Then, we have that

$$\langle s^z | \Psi_s \rangle = J_{ss}(s^z) \det(\phi_{r_\uparrow,\alpha}) \det(\phi_{r_\downarrow,\alpha}), \tag{15}$$

where $\phi_{r_\sigma,\alpha}$ are the $N/2$ (spin-independent) lowest-energy orbitals of the auxiliary Hamiltonian (13), labeled by the index α and evaluated on the positions of up ($r_\uparrow$) and down spins ($r_\downarrow$) in the configuration $|s^z\rangle$; $J_{ss}(s^z)$ is the value of the operator $\mathcal{J}_{ss}$ on the configuration $|s^z\rangle$.

The parameters, which are optimized in order to minimize the variational energy (5), are given by the hoppings ($t_{i,j}$) of the auxiliary Hamiltonian, the centers of the Gaussians ($\vec{z}_i$), and the Jastrow pseudopotentials [$v_{ss}(\|\vec{r}_i - \vec{r}_j\|)$, $v_{sp}^X(\|\vec{r}_i - \vec{r}_j\|)$, and $v_{sp}^Y(\|\vec{r}_i - \vec{r}_j\|)$] at all inequivalent lattice distances. The optimization procedure is performed by using the stochastic reconfiguration method [54].

B. Lattice distortions and supercells

A challenging aspect of this study is determining the most favorable lattice distortions that are induced by the spin-phonon interaction and could represent potential instabilities of the Dirac spin-liquid state. Instead of considering a variational phonon *Ansatz* $|\Psi_p\rangle$ with a fixed phonon momentum and a certain polarization (as done in Ref. [47]), we apply a more general approach in which we scan through several supercells that can accommodate different patterns of distortions. Within this method, the variational parameters $t_{i,j}$ [Eq. (13)] and $\vec{z}_i$ [Eq. (10)] are taken to be translationally invariant with respect to the chosen supercell. Thus, for a supercell of N_s sites, $2N_s$ independent nearest-neighbor hoppings and N_s $\vec{z}_i$ parameters are optimized. This strategy allows us to describe combinations of phonon modes with different momenta and polarizations.

We consider supercells of various sizes and shapes. They are defined by means of three distinct sets of vectors, $\vec{a}_i$, $\vec{b}_i$, and $\vec{c}_i$ ($i = 1, 2$), shown in Fig. 1. The supercells constructed by the a-vectors are denoted as $(m, n)_a$ ($m, n \in \mathbb{N}$) and defined

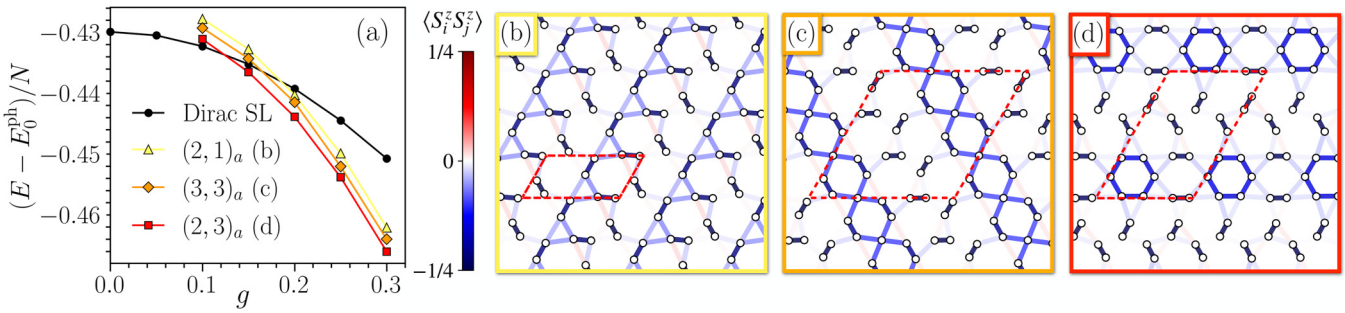

FIG. 2. Results of the calculations on the $(6, 6)_a$ cluster ($N = 108$ sites). In panel (a) the energies (per site) of the Dirac spin liquid (SL) and different valence-bond ordered states are shown as a function of the spin-phonon coupling g. The zero-point energy of the phonon Hamiltonian, $E_0^{\rm ph} = N\omega$, has been subtracted. The patterns of distortions associated with the various valence-bond ordered states are shown in panels (b), (c), and (d), as obtained within the $(2, 1)_a$, $(3, 3)_a$, and $(2, 3)_a$ supercells, respectively. The color of the bonds between sites i and j represents the value of the spin-spin correlations $\langle S_i^z S_j^z \rangle$ (at $g = 0.3$). The dashed lines delimit the supercells.

by the vectors $m\vec{a}_1$ and $n\vec{a}_2$. An analogous notation is used for the supercells constructed by the $\vec{b}_i$ and $\vec{c}_i$ vectors. We note that the $(m, n)_{a,b,c}$ supercells contain $3m \times n$, $9m \times n$, and $6m \times n$ sites, respectively. We scan several supercells described by these vectors, up to a size of 48 sites. The full cluster, on which numerical calculations are performed, will also be denoted by a similar notation. The three families of supercells are chosen because they represent simple geometries that can be fitted inside the finite-size clusters which are accessible to numerical simulations. In addition, the supercells defined by $\vec{a}_i$ or $\vec{b}_i$ vectors fulfill all the point-group symmetries of the original kagome lattice if $m = n$, while the one defined by $\vec{c}_i$ vectors has been discussed in Ref. [7].

For what concerns the fermionic variational state, we initialize the hoppings of the auxiliary Hamiltonian $\mathcal{H}_0$ in the vicinity of one of the four $U(1)$ symmetric spin liquids of the kagome lattice [55]. Specifically, the initial signs of the hopping parameters reproduce the 0 and/or π fluxes through the triangular and hexagonal plaquettes which characterize the different $U(1)$ spin liquids [55]. The idea behind this approach is motivated by the fact that a symmetric spin liquid can serve as a parent state of certain valence-bond solid instabilities [23,29–31,37,47]. However, since all hopping parameters within the supercell are independently optimized, they can take any value upon energy minimization and thus change the fluxes from their initial values.

III. RESULTS

We study the model of Eq. (1) for $\omega/J = 1$ and different values of the spin-phonon coupling g. Throughout the paper, we set $J = 1$ to fix the energy scale of the problem. At $g = 0$ the lattice is undistorted and the optimal variational state is given by the $U(1)$ Dirac spin-liquid state [20,21]. Turning on the spin-phonon interaction, we observe the appearance of several competing valence-bond ordered states, whose energies eventually beat that of the Dirac spin liquid for large values of g. The main findings of this paper can be summarized in three points: (i) the Dirac spin-liquid state is *stable* for small values of the spin-phonon interaction; (ii) the valence-bond ordered states which provide the lowest energy for large g are characterized by the appearance of hexagonal plaquettes with strong spin-spin correlations; (iii) the transition between the Dirac spin liquid and the best distorted states is of first order.

We begin the discussion by looking at the results obtained on the $(6, 6)_a$ cluster (with $N = 108$ sites), which exemplify the main observations outlined above. For the sake of clarity, we restrict our analysis to $(m, n)_a$ supercells. As shown in Fig. 2(a), for $g \lesssim 0.1$, the Dirac spin liquid gives the best variational energy, but several metastable valence-bond solids with finite distortions can be stabilized within different supercells. When the spin-phonon coupling is sufficiently strong, all these dimerized states become lower in energy than the Dirac spin liquid. The different distortions are shown in Figs. 2(b)–2(d), where the color of the bonds between neighboring sites represents the value of the spin-spin correlations. The higher-energy distorted state [$(2, 1)_a$ in Fig. 2(b)] is essentially made of dimers that form stripes along a_2. The lowest-energy state, instead, is obtained by the $(2, 3)_a$ supercell [Fig. 2(d)] and, in addition to stripes of alternating dimers, shows the appearance of hexagonal plaquettes with strong antiferromagnetic sides. We dub these rotationally symmetric plaquettes *perfect hexagons*. This terminology is borrowed from studies concerning (hard-core) dimer coverings on the kagome lattice, where perfect hexagons are hexagonal plaquettes, which host three dimers and are surrounded by empty triangular plaquettes [6–8,11,16]. In the case of hard-core dimers, due to geometrical constraints, the maximum density of perfect hexagons among hexagonal plaquettes is found to be 1/6, i.e., 1 every 18 sites. The $(2, 3)_a$ valence-bond solid in Fig. 2 is analogous to the 18-site dimer covering found by Marston and Zeng within a large-N expansion of the kagome antiferromagnet, which shows the maximum density of perfect hexagons [6]. The difference lies in the fact that in the present case, in the absence of the hard-core dimer constraint, perfect hexagons possess six edges with equal spin-spin correlations, instead of having three strong and three weak bonds. It is worth mentioning that an intermediate energy state is found by considering the $(3, 3)_a$ supercell. As shown in Fig. 2(c), this valence-bond solid is characterized by parallel stripes of dimers which are connected by relatively strong antiferromagnetic correlations, forming lines of hexagons. We note,

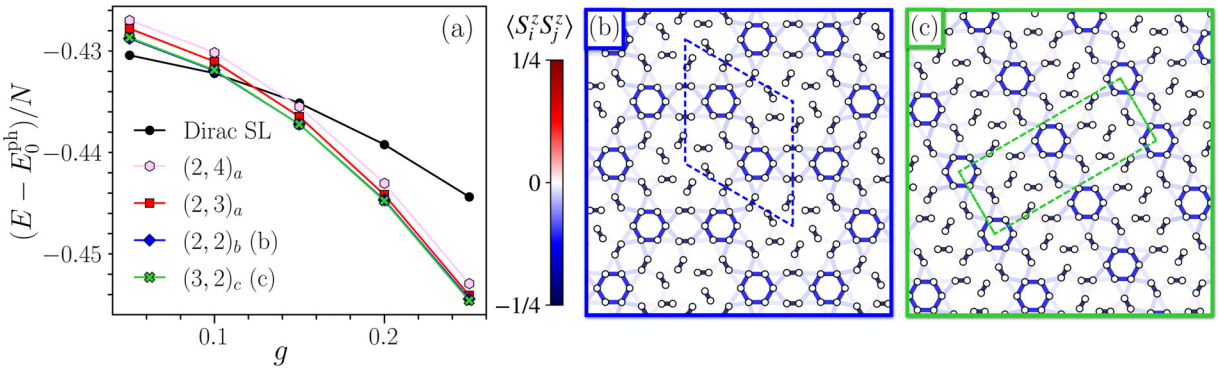

FIG. 3. The same as in Fig. 2 for calculations on the $(12, 12)_a$ cluster ($N = 432$ sites). Panel (a) shows the energies (per site) of the Dirac spin liquid (SL) and different valence-bond solids with perfect hexagons. Panels (b) and (c) show the distortions and spin-spin correlations (at $g = 0.3$) of the $(2, 2)_b$ and $(3, 2)_c$ supercells, respectively.

however, that these hexagons are not perfect, as their edges do not possess equally strong spin-spin correlations.

The preliminary results on the $(6, 6)_a$ cluster already suggest that a large density of perfect hexagons turns out to be the distinguishing hallmark of the best dimerized states of the spin-phonon model (1). For the complete search of possible patterns of distortions, we carried out several calculations on finite-size clusters of various shapes that can accommodate different supercells. The lowest-energy distortions found by this analysis display perfect hexagons in their spin-spin correlation patterns. The energies of these states can be compared by performing calculations on the $(12, 12)_a$ cluster (with $N =$ 432 sites), which can accommodate all the optimal supercells we identified. The results are summarized in Fig. 3, where different patterns with perfect hexagons are compared. Similarly to what has been previously discussed, we find the Dirac spin liquid to be stable to dimerization until a certain critical value of the spin-phonon coupling is reached ($g_c \approx 0.1$). For larger values of g, the lowest-energy states are given by the $(2, 2)_b$ and $(3, 2)_c$ supercells, both containing 36 sites. The lattice distortions and the relative spin-spin correlations of these states are shown in Figs. 3(b) and 3(c) and display the maximal density of perfect hexagons (two per supercell, i.e., 1 every 18 sites). Both these patterns have been discussed in several works as possible ground states of spin (or quantum dimer) models on the kagome lattice [6–9,11,16,23,56,57]. The valence-bond order of Fig. 3(b) shows a honeycomb structure of perfect hexagons, which are arranged around weak hexagonal plaquettes surrounded by a *pinwheel* pattern of dimers. Previous studies on kagome Heisenberg models showed that this valence-bond solid can be favored by a ferromagnetic second-neighbor coupling [23]. The distortion in Fig. 3(c), instead, is characterized by parallel stripes of perfect hexagons [7]. On the $(12, 12)_a$ cluster, the energies obtained by the two 36-sites supercells, $(2, 2)_b$ and $(3, 2)_c$, are slightly lower than that of the 18-sites supercell $(2, 3)_a$ of Fig. 2(d), at least for small values of the spin-phonon coupling. It is not possible, instead, to draw definitive conclusions about which of the two 36-sites valence-bond orders is better than the other, as the relative energy difference is very small and difficult to resolve within stochastic and optimization uncertainties. Still, it can be clearly stated that a large density of perfect hexagons is crucial to obtain the lowest energies. Indeed, similarly to the correlation pattern in Fig. 2(d), the valence-bond state obtained with the $(2, 4)_a$ supercell is also characterized by perfect hexagons separated by stripes of alternating dimers (not shown). However, it possesses a lower density of perfect hexagons, i.e., 1 every 24 sites, and its energy is found to be consistently higher than the states with maximal density, as shown in Fig. 3(a).

The transition between the Dirac spin liquid and the valence-bond-solid states appears to be of first order. This conclusion is motivated by two different observations. On the one hand, the dimerized states can be stabilized as metastable states in the region where the Dirac spin liquid gives the lowest-energy variational *Ansatz*. On the other hand, the analysis of the fluxes threading the elementary plaquettes of the lattice suggests that the valence-bond solids with perfect hexagons cannot be smoothly connected to the Dirac spin-liquid state. Indeed, we find that the product of hoppings around a perfect hexagon always produces 0-flux, which is incompatible with the π-flux threading the hexagonal plaquettes in the Dirac spin-liquid *Ansatz*. We also observe that the hexagons that lie right between two perfect hexagons (and possess two dimers at opposite edges) are always threaded by flux π. No general conclusions can be drawn for the fluxes of the other hexagonal plaquettes of the lattice.

Starting from the results of the unbiased optimization of all the hopping parameters, we found a simpler parametrization for the *Ansatz* of the 36-sites valence-bond solid defined by the $(2, 2)_b$ supercell [Fig. 3(b)]. Indeed, the number of independent hoppings can be narrowed down from 72 to 4, without worsening the variational energy. However, as previously mentioned, the choice of the signs of the hoppings on the different bonds is crucial and induces a specific flux pattern, shown in Fig. 4. We make use of this simplified variational *Ansatz* to perform a numerical experiment to understand why the system prefers to form distortions with perfect hexagons with a rotationally symmetric pattern of correlations, instead of creating strong dimers on three edges. For this purpose, we start from the variational *Ansatz* in Fig. 4, and we force the hoppings on the even/odd edges of the perfect hexagons to take values $1 + \delta t$ and $1 - \delta t$, respectively. The remaining hoppings are optimized, together

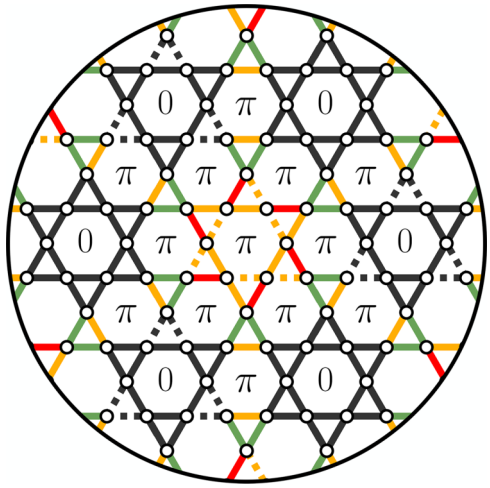

FIG. 4. Fermionic hoppings in the minimal variational *Ansatz* for the $(2, 2)_b$ valence-bond solid. Bonds of different colors correspond to (four) independent absolute values of the hopping parameters. Solid and dashed lines denote positive and negative signs of the hopping, respectively. The fluxes threading the hexagonal plaquettes are reported and compatible with those observed in Ref. [23]. Perfect hexagons can be recognized as the ones with zero flux.

with the other variational parameters. As a result, we are able to draw an energy landscape as we smoothly tune the symmetric hexagons ($\delta t = 0$) into plaquettes with three dimers ($\delta = 1$). Two inequivalent dimerizations can be considered, since the supercell contains two perfect hexagons. The resulting energy loss is reported in Fig. 5, where both the total energy and the contribution from the free phonon Hamiltonian $\mathcal{H}_{\text{ph}}$ are shown. The latter is found to be a small fraction of the total energy loss. Therefore, we conclude that the tendency to form symmetric perfect hexagons (instead of disconnected dimers) is driven by the spin-phonon part of the Hamiltonian.

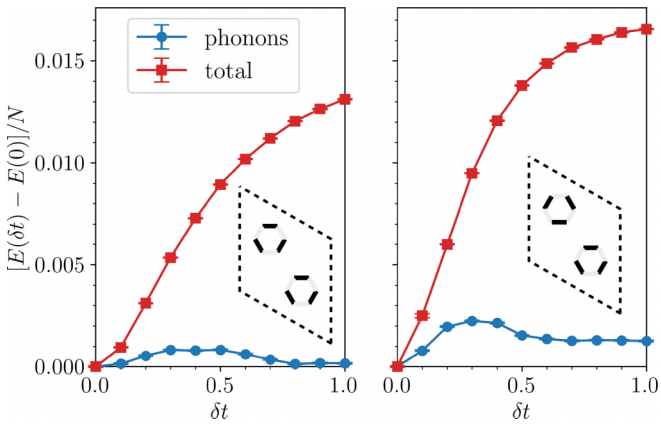

FIG. 5. Energy loss due to forcing a dimerization of the perfect hexagons in the variational *Ansatz* of the $(2, 2)_b$ valence-bond solid (Fig. 4). The total energy loss (red squares) is plotted alongside the contribution due to the free phonon Hamiltonian (blue circles), for two inequivalent dimerization patterns (illustrated in the insets). The results are obtained on the $(4, 4)_b$ cluster ($N = 144$ sites) for $g = 0.3$.

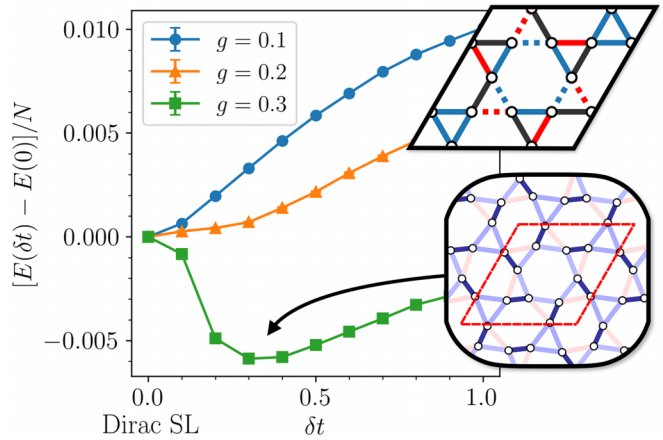

FIG. 6. Energy landscape of the *pinwheel* valence-bond solid *Ansatz* [29] as a function of the tuning parameter δt. The three independent hoppings defining the variational state are shown in the upper inset. Different colors refer to different absolute values, with red/black bonds indicating $|t_{i,j}| = 1 \pm \delta t$. Solid and dashed lines denote, respectively, positive and negative hoppings, which reproduce the characteristic fluxes of the Dirac spin liquid. The lower inset shows the lattice distortions and spin-spin correlations (analogously to Figs. 2 and 3) in the minimum of the variational energy, for $g = 0.3$. The results are obtained on the $(6, 6)_a$ cluster ($N = 108$ sites).

Finally, we mention that finding valence-bond solid instabilities that are continuously connected to the Dirac spin liquid is possible, although they yield higher variational energies than those of the optimal distortions presented above. For example, we constructed a variational *Ansatz* within the $(2, 2)_a$ supercell that reproduces the *pinwheel* valence-bond-solid pattern, which can arise from monopole condensation and lead to a finite gap in the Dirac spectrum [29]. The fermionic Hamiltonian of the variational state contains three hoppings, whose signs yield the characteristic fluxes of the Dirac state, as shown in the upper inset of Fig. 6. The absolute values of the hoppings in red and black are fixed to $1 + \delta t$ and $1 - \delta t$, respectively, while the remaining hopping is optimized, together with all the other variational parameters. In this way, we can draw an energy landscape as a function of the δt parameter, which induces a pinwheel dimerization around the hexagon in the middle of the supercell. As shown in Fig. 6, for small values of the spin-phonon couplings (i.e., $g = 0.1$ and 0.2) the minimum of the energy is found at $\delta t = 0$. Here, the absolute value of the third hopping converges to 1, yielding the Dirac spin liquid, which is then stable with respect to the pinwheel dimerization. On the other hand, when $g = 0.3$, an energy minimum appears for $\delta t \approx 0.3$, indicating that the pinwheel valence-bond-solid state is energetically more convenient than the Dirac spin liquid. The behavior of the energy landscape indicates a second-order transition between the spin liquid and the pinwheel valence-bond solid. Nevertheless, the lowest-energy variational state found by an unbiased optimization in the $(2, 2)_a$ supercell yields the same dimerization pattern of the $(2, 1)_a$ supercell shown in Fig. 2(b). This fact indicates that the *pinwheel* and *diamond* patterns with $(2, 2)_a$ periodicity, proposed in other works as emerging from the monopole condensation of the Dirac spin

liquid on the kagome lattice [29,49], do not actually describe the optimal distortions observed in the present spin-phonon model.

IV. CONCLUSION

In this work, we investigated the potential spin-Peierls instability of the $U(1)$ Dirac spin liquid on the kagome lattice in the presence of a coupling between spins and lattice distortions. Our analysis is based on a spin-phonon Su-Schrieffer-Heeger Heisenberg Hamiltonian in which the antiferromagnetic exchange interaction between the $S = 1/2$ spins depends linearly on relative site displacements, the latter being described by a set of uncoupled harmonic oscillators (Einstein phonons). The full quantum dynamics of the system is taken into account by means of a variational Monte Carlo approach in which both spins and phonons are treated as quantum-mechanical degrees of freedom. Even though we have focused our attention on optical phonons, we do not expect a drastically different scenario when considering an acoustic dispersion. In fact, since all the distortions found in the numerical simulations possess finite momenta, the difference between optical and acoustic dispersions is not expected to play a relevant role. Furthermore, given the substantial energy gain provided by distorted states that cannot be continuously connected to the Dirac spin liquid, it appears rather implausible to obtain a continuous transition between the spin liquid and the valence-bond-solid phases.

Scanning through several supercells and patterns of distortions, we identified the lowest-energy valence-bond ordered states induced by the spin-phonon coupling, which display a large density of perfect hexagons [6], i.e., (rotationally symmetric) hexagonal plaquettes with strong antiferromagnetic correlations at the edges. Other valence-bond ordered states, including those associated with the condensation of monopoles [29,49], are found to be energetically less convenient. The most important outcome of the present study is the observation that the transition towards valence-bond order takes place at finite values of the spin-phonon interaction, which implies that the $U(1)$ Dirac spin liquid is a *stable* phase. Furthermore, the analysis of the variational energies, supported by considerations about the gauge-invariant fluxes characterizing the variational *Ansätze*, indicates that the transition between the Dirac spin liquid and the optimal valence-bond ordered states is of first order.

ACKNOWLEDGMENTS

We thank Y. Iqbal, K. Penc, and J. Schnack for useful discussions. F.F. and R.V. acknowledge support by the Deutsche Forschungsgemeinschaft (DFG, German Research Foundation) for funding through TRR 288–422213477 (Project No. A05).

[1] G. Misguich and C. Lhuillier, *Two-dimensional Quantum Antiferromagnets* (World Scientific, Singapore, 2005), pp. 229–306.
[2] J. T. Chalker and J. F. G. Eastmond, Ground-state disorder in the spin-1/2 kagomé Heisenberg antiferromagnet, Phys. Rev. B **46**, 14201 (1992).
[3] R. R. P. Singh and D. A. Huse, Three-sublattice order in triangular- and kagomé-lattice spin-half antiferromagnets, Phys. Rev. Lett. **68**, 1766 (1992).
[4] P. W. Leung and V. Elser, Numerical studies of a 36-site kagomé antiferromagnet, Phys. Rev. B **47**, 5459 (1993).
[5] S. Sachdev, Kagomé- and triangular-lattice Heisenberg antiferromagnets: Ordering from quantum fluctuations and quantum-disordered ground states with unconfined bosonic spinons, Phys. Rev. B **45**, 12377 (1992).
[6] J. B. Marston and C. Zeng, Spin-Peierls and spin-liquid phases of Kagomé quantum antiferromagnets, J. Appl. Phys. **69**, 5962 (1991).
[7] P. Nikolic and T. Senthil, Physics of low-energy singlet states of the kagome lattice quantum Heisenberg antiferromagnet, Phys. Rev. B **68**, 214415 (2003).
[8] R. R. P. Singh and D. A. Huse, Ground state of the spin-1/2 kagome-lattice Heisenberg antiferromagnet, Phys. Rev. B **76**, 180407(R) (2007).
[9] D. Poilblanc and G. Misguich, Competing valence bond crystals in the kagome quantum dimer model, Phys. Rev. B **84**, 214401 (2011).
[10] R. R. P. Singh and D. A. Huse, Triplet and singlet excitations in the valence bond crystal phase of the kagome lattice Heisenberg model, Phys. Rev. B **77**, 144415 (2008).
[11] D. Poilblanc, M. Mambrini, and D. Schwandt, Effective quantum dimer model for the kagome Heisenberg antiferromagnet: Nearby quantum critical point and hidden degeneracy, Phys. Rev. B **81**, 180402(R) (2010).
[12] P. Lecheminant, B. Bernu, C. Lhuillier, L. Pierre, and P. Sindzingre, Order versus disorder in the quantum Heisenberg antiferromagnet on the kagomé lattice using exact spectra analysis, Phys. Rev. B **56**, 2521 (1997).
[13] F. Mila, Low-energy sector of the $S = 1/2$ kagome antiferromagnet, Phys. Rev. Lett. **81**, 2356 (1998).
[14] M. Mambrini and F. Mila, RVB description of the low-energy singlets of the spin 1/2 kagomé antiferromagnet, Eur. Phys. J. B **17**, 651 (2000).
[15] A. M. Läuchli, J. Sudan, and R. Moessner, $s = \frac{1}{2}$ kagome Heisenberg antiferromagnet revisited, Phys. Rev. B **100**, 155142 (2019).
[16] C. Zeng and V. Elser, Quantum dimer calculations on the spin-1/2 kagomé Heisenberg antiferromagnet, Phys. Rev. B **51**, 8318 (1995).
[17] H. C. Jiang, Z. Y. Weng, and D. N. Sheng, Density matrix renormalization group numerical study of the kagome antiferromagnet, Phys. Rev. Lett. **101**, 117203 (2008).
[18] S. Yan, D. A. Huse, and S. R. White, Spin-liquid ground state of the $s = 1/2$ kagome Heisenberg antiferromagnet, Science **332**, 1173 (2011).
[19] S. Depenbrock, I. P. McCulloch, and U. Schollwöck, Nature of the spin-liquid ground state of the $s = 1/2$ Heisenberg model on the kagome lattice, Phys. Rev. Lett. **109**, 067201 (2012).
[20] Y. Iqbal, F. Becca, S. Sorella, and D. Poilblanc, Gapless spin-liquid phase in the kagome spin-$\frac{1}{2}$ Heisenberg antiferromagnet, Phys. Rev. B **87**, 060405(R) (2013).

[21] Y. Ran, M. Hermele, P. A. Lee, and X.-G. Wen, Projected-wave-function study of the spin-1/2 Heisenberg model on the kagomé lattice, Phys. Rev. Lett. **98**, 117205 (2007).

[22] X.-G. Wen, Quantum orders and symmetric spin liquids, Phys. Rev. B **65**, 165113 (2002).

[23] Y. Iqbal, F. Becca, and D. Poilblanc, Valence-bond crystals in the kagomé spin-1/2 Heisenberg antiferromagnet: A symmetry classification and projected wave function study, New J. Phys. **14**, 115031 (2012).

[24] Y. Iqbal, F. Becca, and D. Poilblanc, Projected wave function study of Z_2 spin liquids on the kagome lattice for the spin-$\frac{1}{2}$ quantum Heisenberg antiferromagnet, Phys. Rev. B **84**, 020407(R) (2011).

[25] Y.-C. He, M. P. Zaletel, M. Oshikawa, and F. Pollmann, Signatures of Dirac cones in a DMRG study of the kagome Heisenberg model, Phys. Rev. X **7**, 031020 (2017).

[26] W. Zhu, X. Chen, Y.-C. He, and W. Witczak-Krempa, Entanglement signatures of emergent Dirac fermions: Kagome spin liquid and quantum criticality, Sci. Adv. **4**, eaat5535 (2018).

[27] F. Ferrari, A. Parola, and F. Becca, Gapless spin liquids in disguise, Phys. Rev. B **103**, 195140 (2021).

[28] H. J. Liao, Z. Y. Xie, J. Chen, Z. Y. Liu, H. D. Xie, R. Z. Huang, B. Normand, and T. Xiang, Gapless spin-liquid ground state in the $s = 1/2$ kagome antiferromagnet, Phys. Rev. Lett. **118**, 137202 (2017).

[29] X.-Y. Song, C. Wang, A. Vishwanath, and Y.-C. He, Unifying description of competing orders in two-dimensional quantum magnets, Nat. Commun. **10**, 4254 (2019).

[30] M. B. Hastings, Dirac structure, RVB, and goldstone modes in the kagomé antiferromagnet, Phys. Rev. B **63**, 014413 (2000).

[31] M. Hermele, Y. Ran, P. A. Lee, and X.-G. Wen, Properties of an algebraic spin liquid on the kagome lattice, Phys. Rev. B **77**, 224413 (2008).

[32] X.-Y. Song, Y.-C. He, A. Vishwanath, and C. Wang, From spinon band topology to the symmetry quantum numbers of monopoles in Dirac spin liquids, Phys. Rev. X **10**, 011033 (2020).

[33] S.-S. Gong, W. Zhu, L. Balents, and D. N. Sheng, Global phase diagram of competing ordered and quantum spin-liquid phases on the kagome lattice, Phys. Rev. B **91**, 075112 (2015).

[34] F. Kolley, S. Depenbrock, I. P. McCulloch, U. Schollwöck, and V. Alba, Phase diagram of the J_1-J_2 Heisenberg model on the kagome lattice, Phys. Rev. B **91**, 104418 (2015).

[35] Y. Iqbal, F. Ferrari, A. Chauhan, A. Parola, D. Poilblanc, and F. Becca, Gutzwiller projected states for the $J_1 - J_2$ Heisenberg model on the kagome lattice: Achievements and pitfalls, Phys. Rev. B **104**, 144406 (2021).

[36] A. Wietek and A. M. Läuchli, Valence bond solid and possible deconfined quantum criticality in an extended kagome lattice Heisenberg antiferromagnet, Phys. Rev. B **102**, 020411(R) (2020).

[37] D. Kiese, F. Ferrari, N. Astrakhantsev, N. Niggemann, P. Ghosh, T. Müller, R. Thomale, T. Neupert, J. Reuther, M. J. P. Gingras, S. Trebst, and Y. Iqbal, Pinch-points to half-moons and up in the stars: The kagome skymap, Phys. Rev. Res. **5**, L012025 (2023).

[38] M. C. Cross and D. S. Fisher, A new theory of the spin-Peierls transition with special relevance to the experiments on TTFCuBDT, Phys. Rev. B **19**, 402 (1979).

[39] E. Pytte, Peierls instability in Heisenberg chains, Phys. Rev. B **10**, 4637 (1974).

[40] G. S. Uhrig, Nonadiabatic approach to spin-Peierls transitions via flow equations, Phys. Rev. B **57**, R14004 (1998).

[41] R. J. Bursill, R. H. McKenzie, and C. J. Hamer, Phase diagram of a Heisenberg spin-Peierls model with quantum phonons, Phys. Rev. Lett. **83**, 408 (1999).

[42] A. W. Sandvik and D. K. Campbell, Spin-Peierls transition in the Heisenberg chain with finite-frequency phonons, Phys. Rev. Lett. **83**, 195 (1999).

[43] F. Ferrari, R. Valentí, and F. Becca, Variational wave functions for the spin-Peierls transition in the su-Schrieffer-Heeger model with quantum phonons, Phys. Rev. B **102**, 125149 (2020).

[44] M. Ye, R. M. Fernandes, and N. B. Perkins, Phonon dynamics in the Kitaev spin liquid, Phys. Rev. Res. **2**, 033180 (2020).

[45] A. Metavitsiadis, W. Natori, J. Knolle, and W. Brenig, Optical phonons coupled to a Kitaev spin liquid, Phys. Rev. B **105**, 165151 (2022).

[46] S. Singh, P. P. Stavropoulos, and N. B. Perkins, Phonon dynamics in the generalized Kitaev spin liquid, Phys. Rev. B **107**, 214428 (2023).

[47] F. Ferrari, R. Valentí, and F. Becca, Effects of spin-phonon coupling in frustrated Heisenberg models, Phys. Rev. B **104**, 035126 (2021).

[48] J. Richter, O. Derzhko, and J. Schulenburg, Magnetic-field induced spin-Peierls instability in strongly frustrated quantum spin lattices, Phys. Rev. Lett. **93**, 107206 (2004).

[49] U. F. P. Seifert, J. Willsher, M. Drescher, F. Pollmann, and J. Knolle, Spin-Peierls instability of the U(1) Dirac spin liquid, arXiv:2307.12295 [cond-mat.str-el].

[50] W. P. Su, J. R. Schrieffer, and A. J. Heeger, Solitons in polyacetylene, Phys. Rev. Lett. **42**, 1698 (1979).

[51] F. Ferrari, F. Becca, and R. Valentí, Charge density waves in kagome-lattice extended Hubbard models at the van Hove filling, Phys. Rev. B **106**, L081107 (2022).

[52] A. A. Abrikosov, Electron scattering on magnetic impurities in metals and anomalous resistivity effects, Phys. Phys. Fiz. **2**, 5 (1965).

[53] L. Savary and L. Balents, Quantum spin liquids: A review, Rep. Prog. Phys. **80**, 016502 (2017).

[54] S. Sorella, Wave function optimization in the variational Monte Carlo method, Phys. Rev. B **71**, 241103(R) (2005).

[55] Y.-M. Lu, Y. Ran, and P. A. Lee, Z_2 spin liquids in the $s = \frac{1}{2}$ Heisenberg model on the kagome lattice: A projective symmetry-group study of Schwinger fermion mean-field states, Phys. Rev. B **83**, 224413 (2011).

[56] G. Evenbly and G. Vidal, Frustrated antiferromagnets with entanglement renormalization: Ground state of the spin-$\frac{1}{2}$ Heisenberg model on a kagome lattice, Phys. Rev. Lett. **104**, 187203 (2010).

[57] Y. Huh, M. Punk, and S. Sachdev, Vison states and confinement transitions of Z_2 spin liquids on the kagome lattice, Phys. Rev. B **84**, 094419 (2011).